

A review on membrane distillation in process engineering: design and exergy equations, materials and wetting problems

Stefano Capizzano¹, Mirko Frappa¹, Francesca Macedonio (✉)¹, Enrico Drioli (✉)^{1,2,3}

¹ Institute of Membrane Technology, National Research Council of Italy, Rende 87036, Italy

² Department of Environmental Engineering, University of Calabria, Rende, Italy

³ Nanjing Tech University, College of Chemical Engineering, Nanjing 211816, China

© Higher Education Press 2021

Abstract One of the problems that most afflicts humanity is the lack of clean water. Water stress, which is the pressure on the quantity and quality of water resources, exists in many places throughout the World. Desalination represents a valid solution to the scarcity of fresh water and several technologies are already well applied and successful (such as reverse osmosis), producing about 100 million $\text{m}^3 \cdot \text{d}^{-1}$ of fresh water. Further advances in the field of desalination can be provided by innovative processes such as membrane distillation. The latter is of particular interest for the treatment of waste currents from conventional desalination processes (for example the retentate of reverse osmosis) as it allows to desalt highly concentrated currents as it is not limited by concentration polarization phenomena. New perspectives have enhanced research activities and allowed a deeper understanding of mass and heat transport phenomena, membrane wetting, polarization phenomena and have encouraged the use of materials particularly suitable for membrane distillation applications. This work summarizes recent developments in the field of membrane distillation, studies for module length optimization, commercial membrane modules developed, recent patents and advancement of membrane material.

Keywords membrane distillation, recent developments, heat and mass transfer, wetting, membrane material

1 Introduction

Water shortage affects at least one billion people on earth

Received April 15, 2021; accepted August 12, 2021

E-mails: f.macedonio@itm.cnr.it (Macedonio F), e.drioli@itm.cnr.it (Drioli E)

and the trend does not seem to stop because of the growing demand of water for domestic, agricultural and industrial use [1]. It has been estimated that almost 6 billion people will suffer from this plague by 2050 [2]. Desalination represents a valid solution to the scarcity of fresh water [3]. Over time, different desalination technologies have been adopted: multi-stage flash distillation (MSF), multiple-effect distillation (MED), mechanical vapor compression (MV), reverse osmosis (RO), nanofiltration (NF) and membrane distillation (MD) [4]. In recent decades, membrane technologies (in particular RO and NF) have replaced thermal-based technologies (such as MSF and MED) with high energy consumption. About 90% of the desalinated water is produced by RO nowadays [5]. MD is a cutting-edge technology for water desalination that is arousing an ever-increasing interest worldwide. As shown in Fig. 1, the number of MD publications has grown considerably since 1998. In MD operations, water evaporates at the feed/membrane interface and diffuses through non-wetted pores to the permeate side under the action of a vapor pressure gradient. The membrane, interposed between the liquid and the vapor phase, prevents any liquid-vapor mixing. The separation mechanism of MD retains all nonvolatile solutes on the feed side so that fresh water is collected on the permeate side. MD is suitable for the separation of highly concentrated salty solutions, e.g., brines from RO installations, produced water and industrial wastewaters. It can be considered as a hybrid membrane and thermal desalination [6]. Historically, different thermal processes have been used in desalination: MSF, MED and TVC (thermal vapor compression). However, since the fifties of the last century, they have been replaced by more efficient membrane processes that make use of electric energy including, in particular, RO [7]. Among the advantages of MD, the ability to work at low temperatures and pressures, the reduced footprint of the plant, the low capital costs

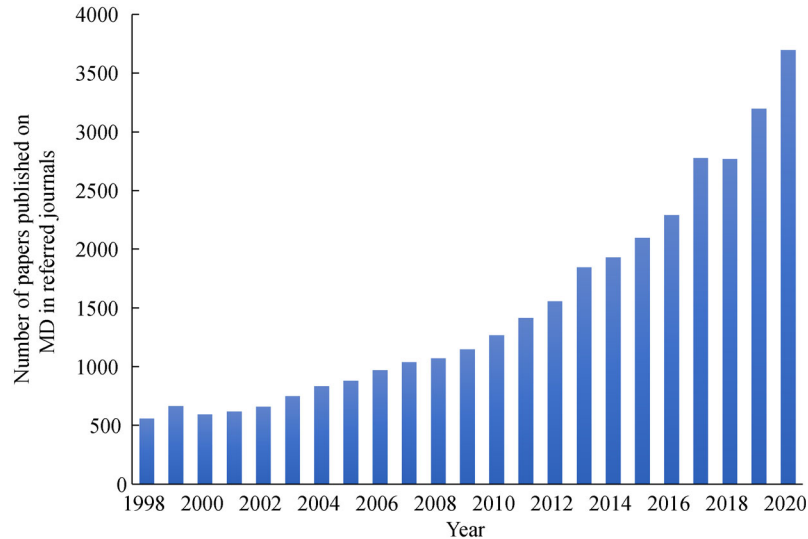


Fig. 1 Growth rate of MD publications up to December 31, 2020 (according to the search results of Science Direct using “membrane distillation” as keyword).

compared to conventional distillation processes and the almost total absence of flux limitations due to concentration polarization must be considered. Unfortunately, the MD permeate flux is a few times lower than that obtained in RO [8]. With the aim of achieving a zero-liquid discharge in desalination, the concept of membrane crystallization (MCr) has been introduced by Drioli and his colleagues in recent times [9–13]. This new salt water treatment technology shares the same separation/concentration mechanism with MD. It is considered as an extension of MD because it concentrates the solution up to the supersaturation state to recover valuable ions from

feed solution. As well as for MD, the driving force of MCr is not significantly affected by the concentration polarization phenomenon. This implies that high recovery factors and concentrations can be reached in MCr operations, as opposed to RO [14]. The production rate of MCr publication (Fig. 2) is, at least for now, markedly lower than that on MD, showing that although this technology has a great potential, it is not yet fully mature.

Only in recent years the supply of membranes and/or membrane modules for MD has become more pronounced and differentiated. Table 1 (modified from [15]) lists the characteristics of the commercial membranes applied in

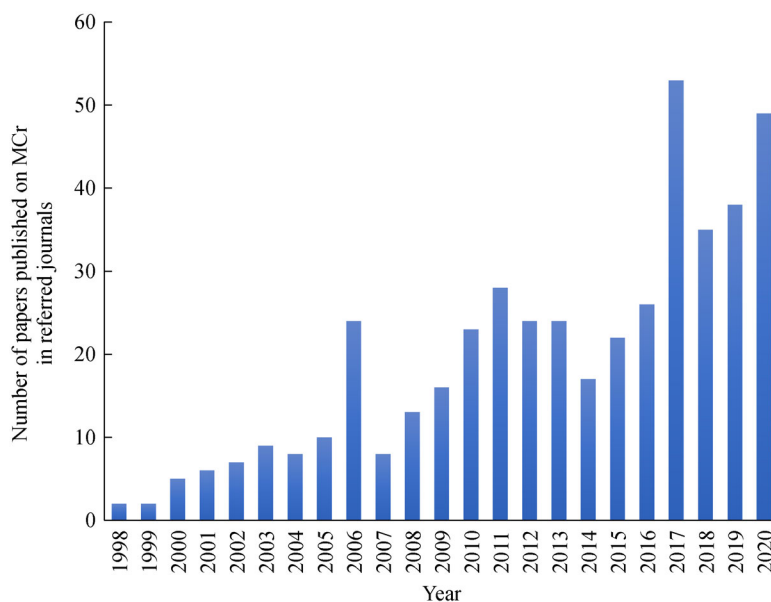


Fig. 2 Growth rate of MCr publications up to December 31, 2020 (according to the search results of Science Direct using “membrane crystallization” as keyword).

Table 1 Commercial membranes used in MD application ^{a)}

| Membrane trade name or details about module configuration | Material | Manufacturer | $\delta/\mu\text{m}$ | $\varepsilon/\%$ | LEF_w/kPa | Ref. |
|---|--|-----------------------|--|---------------------------------------|--------------------|---------|
| Plate and frame module | Polytetrafluoroethylene (PTFE) | Scarab development AB | 200 | 80% | – | [17] |
| Spiral wound module | Membrane in PTFE supported on polypropylene (PP) | Solar spring GmbH | 70 for PTFE, 280 for the support in PP | 80 for PTFE, 50 for the support in PP | – | [18,19] |
| Spiral wound module | Low-density polyethylene (LDPE) | Aquastill BV | 76 | 85 | – | [20] |
| Plate and frame module | PTFE | Memsys GmbH | 20 μm (200 μm if including the supporting layer) | 70–75 | – | [21] |
| Hollow fiber membrane modules | Polyvinylidene fluoride (PVDF) | Econity | – | – | – | |
| TF200 | PTFE/PP | Gelman | 178 | 80 | 282 | |
| TF450 | PTFE/PP | Gelman | 178 | 80 | 138 | [22–24] |
| TF1000 | PTFE/PP | Gelman | 178 | 80 | 48 | |
| PT20 | PTFE/PP | Gore | 64 \pm 5 | 90 \pm 1 | 368 \pm 1 | [22] |
| PT45 | PTFE/PP | Gore | 77 \pm 8 | 89 \pm 4 | 288 \pm 1 | [22] |
| TS1.0 | PTFE/PP | Osmonics Corp. | 175 | 70 | – | |
| TS22 | PTFE/PP | Osmonics Corp. | 175 | 70 | – | [23] |
| TS45 | PTFE/PP | Osmonics Corp. | 175 | 70 | – | |
| Taflen | PTFE/PP | Gelman | 60 | 50 | – | |
| FGLP | PTFE/PP | Millipore | 130 | 70 | 280 | |
| FHLP | PTFE/PP | Millipore | 175 | 85 | 124 | |
| GVHP | PVDF | Millipore | 110 | 75 | 204 | |
| PV22 | PVDF | Millipore | 126 \pm 7 | 62 \pm 2 | 229 \pm 3 | [22,25] |
| PV45 | PVDF | Millipore | 116 \pm 9 | 66 \pm 2 | 110 \pm 4 | |
| HVHP (Durapore) | PVDF | Millipore | 140 | 75 | 105 | |
| GVSP | PVDF | Millipore | 108 | 80 | – | [23] |
| GORE | PTFE | Gore | 64 | 90 | 368 | |
| GORE | PTFE | Gore | 77 | 89 | 288 | |
| Tecknokrma | PTFE | Tecknokrma | – | 80 | – | |

(Continued)

| Membrane trade name or details about module configuration | Material | Manufacturer | $\delta/\mu\text{m}$ | $\varepsilon/\%$ | LEP_w/kPa | Ref. |
|---|-------------------|----------------------|----------------------|------------------|--------------------|---------|
| Teknokrama | PTFE | Teknokrama | – | 80 | – | |
| Teknokrama | PTFE | Teknokrama | – | 80 | – | |
| G-4.0-6-7 | PTFE | GoreTex Sep GmbH | 100 | 80 | 463 | |
| Sartorius | PTFE | Sartorius | 70 | 70 | – | |
| MD080CO2N | PP | Enka Microdyn | 650 | 70 | – | |
| MD020TP2N | PP | Enka Microdyn | 1550 | 70 | – | [22,23] |
| Accurel® | PP | Enka A.G. | 400 | 74 | – | |
| Celgard X-20 | PP | Hoechst Celanese Co. | 25 | 35 | – | |
| Accurel® S6/2 | PP | Akzo Nobel | 450 | 70 | 140 | [22] |
| Enka | PP | Sartorius | 100 | 75 | – | |
| Enka | PP | Sartorius | 140 | 75 | – | [23] |
| 3MA | PP | 3M Corporation | 91 | 66 | – | |
| 3MB | PP | 3M Corporation | 81 | 76 | – | |
| 3MC | PP | 3M Corporation | 76 | 79 | – | |
| 3MD | PP | 3M Corporation | 86 | 80 | – | |
| 3ME | PP | 3M Corporation | 79 | 85 | – | |
| Membrana | PP | Membrana, Germany | 91 | – | – | |
| PP22 | PP | Osmionics Corp. | 150 | 70 | – | |
| Metricel | PP | Gelman | 90 | 55 | – | |
| Celgard 2400 | PP | Hoechst Celanese Co. | 25 | 38 | – | |
| Celgard 2500 | PP | Hoechst Celanese Co. | 28 | 45 | – | |
| EHF270FA-16 | polyethylene (PE) | Mitsubishi | 55 | 70 | – | |

a) δ : membrane thickness; ε : porosity; LEP_w : liquid entry pressure of water.

MD processes; some of them have been fabricated for different membrane operations and subsequently adapted to MD applications, other have been suitably developed for the MD technique (such as the membrane modules manufactured by Econity, TNO, Scarab, Solar Spring GmbH, Aquastill BV, Memsys GmbH). The existing commercial modules are mainly based on the use of flat membranes in spiral wound and plate and frame configurations. Some attempts were made by KmX Corporation (Canada) to produce hollow fiber membrane-based modules, but not many information about their properties and performance are provided [16]. A successful effort was done by Econity whose hollow fiber membrane modules have been recently used in the seawater reverse osmosis-membrane distillation (SWRO-MD) pilot plant built at the institute of Fisheries Science in Pukyong National University (located in Busan, South Korea) in the framework of the GMVP project.

All the membranes listed in Table 1 are made of polymeric materials. In the last years, ceramic membranes are being prepared for MD applications, too. The main advantages in using ceramic membranes are their greater resistance to strong solvents (such as acids) and mechanical strength compared to polymeric materials. However, the ceramic membranes have high thermal conductivity and are inherently hydrophilic in nature and therefore, in principle, not suitable for MD applications. According to Al-Obaidani et al. [26], high thermal conductivity is associated with reduced thermal efficiency. The latter can be improved by increasing membrane thickness in order to lower heat losses. Regarding the hydrophilic nature of the ceramic membranes, some attempts have been made to alter it: Picard et al. [27] have reported the application of different fluorinated silanes to render hydrophobic character to various hydrophilic microfiltration and ultrafiltration membranes; Dafinov et al. [28] used alcohol adsorption to modify the hydrophilic surface of commercial γ -alumina membrane. Ko et al. [29] prepared two different hydrophobic ceramic membranes for MD and MCr operations: i) a first membrane was fabricated by coating hydrophobic polymethylsilsesquioxane aerogels on alumina membrane supports via a sol-gel process; ii) a second one was prepared by applying fluoroalkylsilanes (1H, 1H, 2H, 2H-perfluorooctyltriethoxysilane) hydrophobic agent at porous as-sintered alumina hollow fibers. The membranes showed stable hydrophobic character in membrane distillation tests and in the crystallization of NaCl (sodium chloride) and LiCl (lithium chloride). Chen et al. [30] investigated the water flux and salt retention in vacuum membrane distillation of tubular hydrophobic alumina membranes grafted with hexadecyltrimethoxysilane. Among the membranes tested, the most performing one produced a constant water flux of about $30 \text{ kg} \cdot \text{m}^{-2} \cdot \text{h}^{-1}$ and a salt rejection of 99.9%, for a desalination of 1000 min. For what concerns the principal configurations in which MD can be operated, these can be found in Fig. 3:

direct contact membrane distillation (DCMD), air gap membrane distillation (AGMD), sweep gas membrane distillation (SGMD) and vacuum membrane distillation (VMD). Among all, DCMD is the simplest and most studied configuration in which a hot feed and a cold permeate flow from opposite sides of the membrane [31]. The AGMD works by means of the interposition of an air gap between the membrane and the condensation surface while SGMD employs a sweeping gas as a vapor carrier on the permeate side [32]. Finally, in VMD the vapor phase is vacuumed from the liquid through the membrane, being condensed in another device. The merits and demerits related to these configurations are listed in Table 2. The thermal and concentration profiles of each configuration are presented below in Section 3. The most recent patents related to MD are reported in Table 3. They concern materials and methods used in membrane preparation and new module designs, aimed at improving the process efficiency and the energy consumption. Several reviews on MD can be found in literature: Drioli et al. [22] presented aspects related to module design, heat and mass transport phenomena, nontraditional fouling and MD applications; Ravi et al. [33] discussed the morphology and the impact on fluid dynamics of surface modified, dual-triple layer and nanocoated membranes, and Yao et al. [35] treated extensively the problems associated with wetting, fouling and strategies to prevent them. This review paper provides information on some of the main areas of interest in MD including design, materials and wetting problems, while no particular attention has been devoted to MD applications (already extensively reported in [22,35]), and MD pilot units (described in detail in [36]). More specifically, it illustrates the optimal characteristics for MD membranes, principal design equations related to the best-known and most used MD configurations, definition and theories on concentration and temperature polarization, results obtained from computer simulation on the optimized module length, exergy analysis, progresses in membrane material, wetting and fouling phenomena, with a reference to experimental observations of wetting due to the interaction between ions and membrane material.

2 Optimal characteristics for MD membranes

MD is a membrane-dependent process because the structural and physicochemical parameters of the membrane strongly determine its efficacy and efficiency. Thickness, porosity, mean pore size, pore distribution and geometry are included among the physical properties of MD membranes while the chemical properties of MD membranes are affected by the chemical treatments, the composition of matrices and the presence of additives and coatings, if any. Both the physical and the chemical properties contribute to the following physicochemical

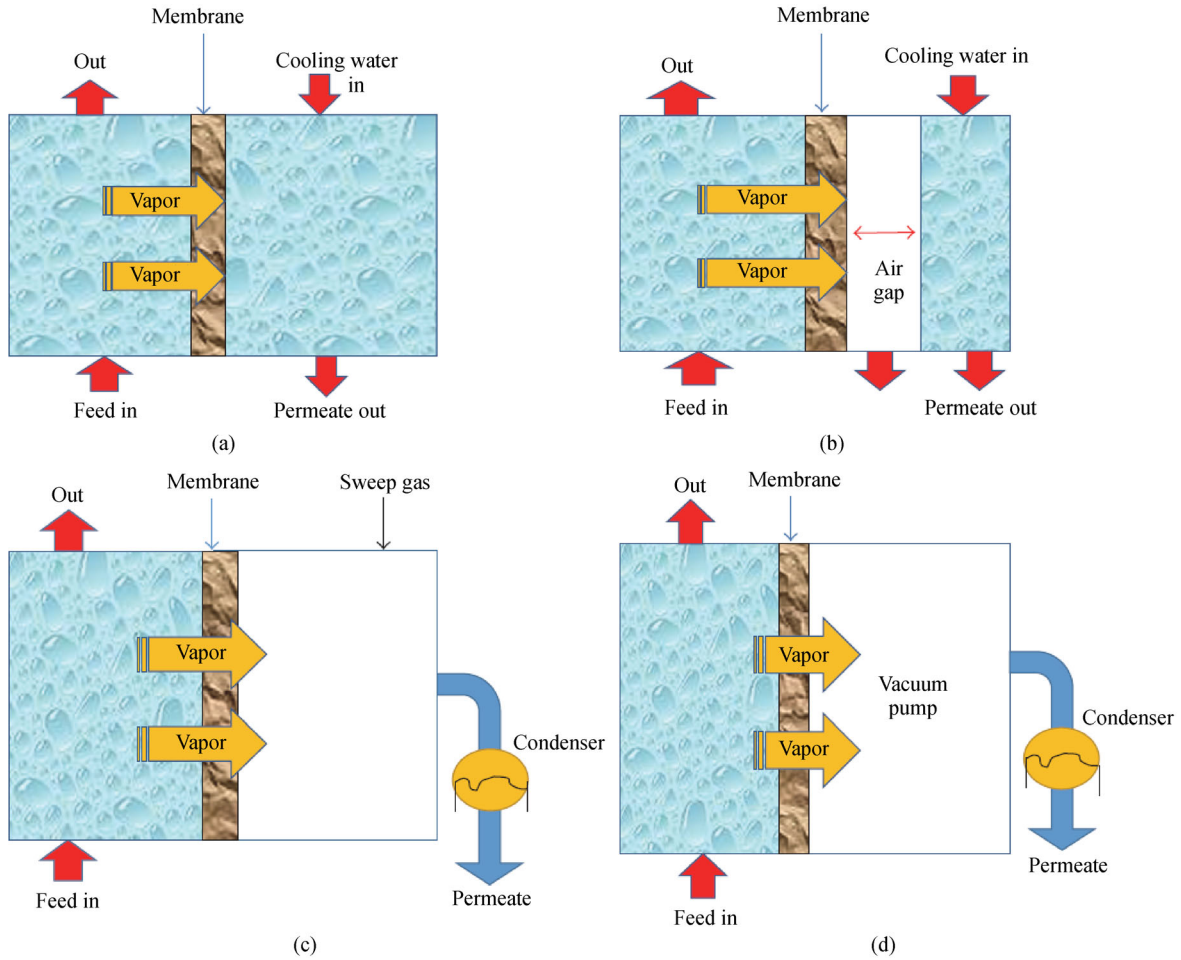


Fig. 3 (a) DCMD; (b) AGMD; (c) SGMD; (d) VMD. Reprinted from ref. [37] (Open access).

parameters: liquid entry pressure (LEP), thermal conductivity, permeability, fouling rate, thermal and chemical stability, mechanical strength and long-term performance. The subsection below focuses on the desired characteristics for MD membranes.

2.1 High liquid entry pressure

LEP_w is the minimum hydrostatic pressure that a feed solution requires to penetrate the hydrophobic membrane [38]. The higher the LEP_w , the lower the tendency to wetting. Franken et al. defined LEP_w as follows [39]:

$$LEP_w = -\frac{2B\gamma_l \cos\theta}{r_{\max}}, \quad (1)$$

where the factor B accounts for geometrical irregularities of pores ($B = 1$ for cylindrical pores), γ_l is the surface tension of water, θ stands for the contact angle between water and the membrane surface and r_{\max} is the radius of the biggest pore of the membrane. To increase LEP_w , membranes must have high contact angles and small pore sizes. According to Wenzel's theory the contact angle is

correlated with surface roughness through Eq. (2) [40,41]:

$$\cos\theta = \frac{r^*(\gamma_{sv} - \gamma_{sl})}{\gamma_{lv}}, \quad (2)$$

in which r^* represents the surface roughness factor, θ is the contact angle, γ_{sv} , γ_{sl} and γ_{lv} are solid/vapor, solid/liquid, liquid/vapor interfacial tensions respectively. It is also noteworthy that if on the one hand a reduction of pore size may lead to an increase of LEP_w , it could reduce the permeate flux up to unacceptable levels.

2.2 High thermal stability and low thermal conductivity

A MD membrane is thermally stable if high temperatures do not degrade or decompose its material. The glass-transition temperature (T_g) and the melting point (T_m) are associated with morphological changes in amorphous and crystalline polymers, respectively. Over T_g , an amorphous material goes from a hard and brittle state to a viscous or rubbery state as the temperature is increased. The value of T_g is determined by the chemical structure of polymers,

Table 2 Advantages and disadvantages of the four most used MD configurations. Adapted with permission from ref. [22], copyright 2015, Elsevier

| Configuration | Advantage | Disadvantage |
|---------------|---|--|
| DCMD | The easiest and simplest configuration to realize practically; flux is more stable than VMD for the feeds with fouling tendency; high gained output ratio [42]; suitable for the removal of volatile components since it was found to give higher selectivity than SGMD and VMD under similar operating conditions [43] | Flux obtained is relatively lower than vacuum configurations under the identical operating conditions; thermal polarization is highest among all the configurations; flux is relatively more sensitive to feed concentration; the permeate quality is sensitive to membrane wetting; suitable mainly for aqueous solutions |
| AGMD | Lower fluxes than the other MD configurations [44]; low thermal losses; integrable with heat recovery systems; no wetting on permeate side; less fouling tendency | Air gap provides an additional resistance to vapors; difficult module design; difficult model due to the involvement of too many variables; lowest gained output ratio [42] |
| SGMD | Thermal polarization is lower; no wetting from permeate side; permeate quality independent of membrane wetting | Additional complexity due to the extra equipment involved; heat recovery is difficult; low flux; pretreatment of sweep gas might be needed |
| VMD | High flux; can be used for recovery of aroma compounds and related substances [45,46]; the permeate quality is stable despite of some wetting; no possibility of wetting from distillate side; thermal polarization if very low | Higher probability of pore wetting; higher fouling; minimum selectivity of volatile components [43]; require vacuum pump external condenser |

mainly the chain flexibility and chain interaction. Table 4 presents the values of T_g for the most common polymers employed in MD. It is evident that PTFE preserves its glassy morphology for a greater temperature range than PE and PP, being its T_g by far greater. T_g is always lower than the melting temperature of the crystalline state of the material, if one exists. The material, thickness and porosity of the membrane influence its thermal behavior. Low thermally conductive membranes are preferable because they reduce the conductive heat losses and the occurrence of thermal polarization phenomena. Thinner membranes are intrinsically more conductive than their thicker counterparts [47]. High porosity lessens the conductive heat losses, since vapor has lower thermal conductivity than the solid membrane material, but enhances permeability too [48–50].

2.3 High permeability

Trans-membrane molar flux (N) can be described by the following equation [51]:

$$N \propto \frac{\psi^\alpha \varepsilon}{\tau \delta}, \quad (3)$$

where ψ^α stands for the average pore size for Knudsen diffusion ($\alpha = 1$) or the average squared pore size for viscous flux ($\alpha = 2$). The other parameters are: the membrane porosity ε , the membrane tortuosity τ and the membrane thickness δ . From the equation above, it is clear that molar flux is directly proportional to membrane pore size and porosity, and inversely proportional to tortuosity and membrane thickness. Even though the molar flux is favored by high porosity and reduced thickness, large pores and thin membranes could induce a flux reduction due to the decrease of LEP and the increase of heat losses. Therefore, it is noticeable that the morphological parameters of Eq. (3) must be optimized in the membrane

design process [52]. A narrow pore distribution is always preferable, being associated with flux uniformity. The optimal values of porosity, pore size and thickness are 80%–90%, 0.5–0.6 and 100–200 μm , respectively [53–55].

2.4 Low fouling rate

Fouling is the deposition of organic and inorganic materials on the surface or in the pores of the membrane. It influences the wettability of the membrane and reduces its performance by lowering the permeate flux because of the decrease of temperature and vapor pressure on the feed side [56]. Fouling is more relevant in pressure driven processes like RO, in which it also occurs in membrane pores. Calcium carbonate and calcium sulfate are common types of inorganic foulants, often referred to as scaling. MD membranes could be exposed to organic foulants such as oil or bio foulants (especially microorganisms), as costal industry effluents and spillages are sometimes dumped into the sea. The main mitigation strategies for this undesirable phenomenon are: pre-filtration (particularly suitable for wastewater with high fouling tendency [57,58]), membrane cleaning (obtainable either with physical processes involving hydraulic, pneumatic, mechanic and electric approaches or by the use of chemicals such as acids, bases, oxidants and surfactants [59]), operating conditions (including temperature, pressure, time, pH [60]), hydrodynamic optimization of the membrane module and modification of the membrane surface (by coating or grafting of special hydrophobic and hydrophilic materials [61] as discussed in Section 9).

2.5 Excellent chemical stability

MD membranes that exhibit excellent chemical stability are more likely to resist chemicals over the long-term. Feed

Table 3 List of MD-related patents published in the period from January 2020 to February 2021

| Patent | Inventor | Remark |
|--|--|--|
| Membrane distillation device with bubble column dehumidifier Publication number: US20200095138A1 Date of patent: Mar. 26, 2020 | Atia Esmail Khalifa Mohamed A. Antar Suhaib M. Alawad | The present disclosure relates to a desalination device comprising a membrane distillation module with a water feed chamber, a CG (carrier gas) chamber, and a hydrophobic microporous membrane configured to separate the water feed chamber and the CG chamber |
| Porous membrane for membrane distillation, and method for operating membrane distillation module Publication number: US20200109070 A1 Date of patent: Apr. 9, 2020 | Tomotaka Hashimoto Hiroyuki Arai Kazuto Nagata Noboru Kubota Hiroki Takezawa Takehito Otoyō | The invention relates to a membrane distillation device, provided with a membrane distillation module including a plurality of hydrophobic porous hollow fiber membranes, and a condenser for condensing water vapor extracted from the module |
| Multistage membrane distillation system for distilled water production Publication number: US20200179877 A1 Date of patent: Jun. 11, 2020 | Atia Esmail Khalifa | The present disclosure relates to a membrane distillation module with a circulating line to circulate a portion of distilled water, which is formed and accumulated in a distillate zone, to enhance a permeate flux of water vapor through a hydrophobic membrane of the membrane distillation module. Various combinations of embodiments of the membrane distillation module are provided |
| Plate-type membrane distillation module with hydrophobic membrane Publication number: US20200179876 A1 Date of patent: Jun. 11, 2020 | Atia Esmail Khalifa | The invention relates to a membrane distillation module with a circulating line to circulate a portion of distilled water, which is formed and accumulated in a distillate zone, to enhance a permeate flux of water vapor through a hydrophobic membrane of the membrane distillation module. Various combinations of embodiments of the membrane distillation module are provided |
| Porous membrane for membrane distillation, membrane module, and membrane distillation device Publication number: US20200179876 A1 Date of patent: Jun. 11, 2020 | Mitsunori Iwamuro Yasuharu Murakami Tatsuya Makino | The object of the present invention is to provide a porous membrane, containing aerogel particles, for membrane distillation excellent in thermal insulation properties |
| Hollow fiber membrane module for direct contact membrane distillation-based desalination Publication number: US20200197867 A1 Date of patent: Jun. 25, 2020 | Kamalesh Sirkar Dhananjay Singh Lin Li Thomas J. McEvoy | The present disclosure has been developed to describe the observed water production rates of a cylindrical cross-flow module containing high-flux composite hydrophobic hollow fiber membranes in multiple brine feed introduction configurations |
| Nanostructured fibrous membranes for membrane distillation Publication number: US20200316504 A1 Date of patent: Oct. 8, 2020 | Benjamin Chu Benjamin S. Hsiao | The present disclosure relates to membranes suitable for use in membrane distillation including nano-fibrous layers with adjustable pore sizes, hydrophobic nanofibrous scaffolds and thin hydrophilic protecting layers that can significantly reduce fouling and scaling problems |
| Hydrophobic polyethylene membrane for use in venting, degassing, and membrane distillation processes Publication number: US20200406201A1 Date of patent: Dec. 31, 2020 | Wai Ming Choi Jad Ali Jaber Vinay Goel Vinay KALYANI Anthony Dennis | The invention relates to polyethylene membranes and with high molecular weight and hydrophobicity, that have been obtained by stretching polyethylene and grafting hydrophobic monomers onto the membrane surface |
| Novel materials and methods for photothermal membrane distillation Publication number: US20210023505 A1 Date of patent: Jan. 28, 2021 | Young-Shin Jun Srikanth Singamaneni Xuanhao Wu Qisheng Jiang | This patent discloses a photothermal distillation membrane comprising a tridecafluoro-1,1,2,2-tetrahydrooctyl-trichlorosilane (FTCS) fluoro-silanized, polydopamine (PDA) coated, PVDF membrane and a process for synthesizing a FTCS-PDA-PVDF membrane |
| Solar thermal membrane distillation system for drinking water production Publication number: US20210017048 A1 Date of patent: Jan. 21, 2021 | Peng Yi Rahamat Ullah Tanvir Shahin Ahmed Suion | This invention relates to a solar distillation device that includes a feed water chamber having an open interior feed water compartment and a feed water inlet to the feed water compartment. The top, the rear wall, and the sides of the distillate chamber include a solar radiation transmissive portion |
| Apparatus for solar-assisted water distillation using waste heat of air conditioners Publication number: US10926223B2 Date of patent: Feb. 23, 2021 | Fahad G. AL-AMRI | The invention presents an apparatus for water purification that includes a MD cell, an air conditioner and a photovoltaic solar collector cell including a transparent photovoltaic cell configured to generate electricity |

solutions contaminated with highly reactive chemicals and treatments such as backwashing or cleaning with solvents could accelerate the degradation process of MD mem-

branes [62]. High operating temperatures can also have a detrimental impact on the structure of polymeric membranes.

Table 4 Glass transition temperature T_g , melting point T_m and thermal conductivity K of polymers

| Polymer | $T_g/^\circ\text{C}$ | Ref. | $T_m/^\circ\text{C}$ | $K/(\text{W}\cdot\text{m}^{-1}\cdot\text{K}^{-1})$ |
|------------------------|----------------------|------|----------------------|--|
| PE | -120 | [65] | 85 to 140 | 0.33 to 0.52 |
| PVDF | -40 | [65] | 155 to 185 | 0.1 to 0.25 |
| PP | -15 | [65] | 165 to 175 | 0.1 to 0.22 |
| PTFE | 126 | [65] | 320 to 330 | 0.25 |
| Polysulfone | 190 | [65] | 185 | 0.26 |
| Hyflon | 192 | [66] | 280 to 290 | 0.20 |
| Polyethersulfone (PES) | 230 | [65] | 230 | 0.13 to 0.18 |
| Polyimide (Kapton) | 300 | [65] | 375 to 401 | 0.10 to 0.35 |

2.6 Excellent mechanical strength

Low mechanical resistance leads to pore collapse and membrane breakage. Sponge-like structures slow down the formation of macrovoids which weaken the mechanical strength of membranes [63]. The presence or not of macrovoids is directly related to the membrane formation process [64].

2.7 Excellent long-term performance

Enhancing the long-term performance of membranes translates into a reduction of operational costs of MD operations. Membrane modification or special coating might be done to enhance the mass transfer through the membrane thus improving the MD performance [67,68]. However, McGaughey et al. [69] found that membranes with surface coatings or active layers are more easily damaged in long-term MD operations. After a prolonged exploitation of MD membranes, flux and salt rejections decrease while the electric conductivity of the obtained distillate increases [70].

3 Mass and heat transfer in MD configurations

In the following section, mass and heat transfer phenomena as well as exergy analysis of principal MD configurations are described.

3.1 DCMD

In DCMD, the total mass resistance (R_{TOT}) can be defined as the sum of the feed resistance (R_f), the membrane resistance (R_m) and the permeate resistance (R_p), as follows [71]:

$$R_{TOT} = R_f + R_m + R_p, \quad (4)$$

where:

$$R_f = \frac{(P_f - P_{fm})}{N}, \quad (5)$$

$$R_m = \frac{(P_{fm} - P_{pm})}{N}, \quad (6)$$

$$R_p = \frac{(P_{pm} - P_p)}{N}, \quad (7)$$

where P_{fm} and P_{pm} are the vapor pressures at the membrane surface on feed and permeate side, respectively. According to the mass transport model chosen, the preferable value of R_m changes accordingly. If the Knudsen model is used, R_m corresponds to:

$$R_m = \frac{\delta\tau RT}{\varepsilon MW_s D_{KA}}, \quad (8)$$

where δ is the membrane thickness, τ the tortuosity factor, R is the universal gas constant, ε the porosity, T the average temperature across the membrane, MW_s the molecular weight of the solvent (water, specifically) and D_{KA} the Knudsen diffusion coefficient that can be calculated as $D_{KA} = 97r \left(\frac{T}{MW_s} \right)^{0.5}$ (in which r is the mean pore size). In accordance with the molecular diffusion model, R_m can be calculated as:

$$R_m = \frac{\delta\tau R P_{ln} T}{\varepsilon MW_s P D_{WA}}, \quad (9)$$

with P_{ln} the long mean partial pressure of air calculated at the membrane surface temperatures, P the total pressure of air and water vapors and D_{WA} the molecular diffusion coefficient that can be calculated as $D_{WA} = 1.19 \times 10^{-4} \frac{T^{1.75}}{P}$. In the event that, in the considered physical system, it is not possible to neglect one of the two models, R_m becomes:

$$R_m = \frac{\delta\tau RT}{\varepsilon MW_s D_{KA}} + \frac{\delta\tau R P_{ln} T}{\varepsilon MW_s P D_{WA}}. \quad (10)$$

The total flux in MD applications is expressed as:

$$N = \frac{P_f - P_p}{R_f + R_m + R_p}, \quad (11)$$

where P_f and P_p are the feed and permeate vapor pressures at bulk, respectively. In general, the transmembrane flux is represented by the following simple correlation:

$$N = C(P_{fm} - P_{pm}), \quad (12)$$

where the permeability C is the membrane mass transfer coefficient for the system whose value is determined by the mass transport model chosen.

Similarly, the heat transfer occurs in three steps: from the feed bulk to the membrane surface (Q_f), through the membrane (Q_m) and from the membrane surface to the bulk of the permeate (Q_p):

$$Q_f = h_f(T_f - T_{fm}), \quad (13)$$

$$\begin{aligned} Q_m &= \frac{K_m}{\delta}(T_{fm} - T_{pm}) + J\lambda \\ &= h_c(T_{fm} - T_{pm}) + h_v(T_{fm} - T_{pm}), \end{aligned} \quad (14)$$

$$Q_p = h_p(T_{pm} - T_p), \quad (15)$$

where h_f and h_p are the heat transfer coefficients for the feed and permeate side obtainable from the general equation $h_i = \frac{Nu_i K_i}{D_h}$ (with Nu the Nusselt number, K the thermal conductivity and D_h , the hydraulic diameter). The latent heat is referred to as λ while K_m stands for the thermal conductivity and can be calculated as:

$$K_m = \varepsilon K_g + (1 - \varepsilon)K_p, \quad (16)$$

with K_g and K_p the thermal conductivity of air and of the specific membrane material considered, respectively.

According to Eq. (14), $h_c = \frac{K_m}{\delta}$ and $h_v = \frac{J\lambda}{(T_{fm} - T_{pm})}$. T_f , T_{fm} , T_p and T_{pm} are the bulk and surface temperatures at feed and permeate side, according to the subscript.

At steady-state:

$$Q_f = Q_m = Q_p, \quad (17)$$

from which the overall heat transfer coefficient can be written as:

$$\begin{aligned} \frac{1}{U} &= \frac{1}{h_f} + \frac{1}{h_c + h_v} + \frac{1}{h_p} \\ &= \frac{1}{h_f} + \frac{1}{\frac{K_m}{\delta} + \frac{J\lambda}{(T_{fm} - T_{pm})}} + \frac{1}{h_p}. \end{aligned} \quad (18)$$

Finally, the total heat transfer across the membrane is

given by:

$$Q = U\Delta T, \quad (19)$$

while the thermal efficiency in MD can be specified as the ratio of latent heat of vaporization to the total (latent and conduction) heat. For DCMD, the thermal efficiency ($T.E.$) can be expressed as:

$$T.E. = \frac{J\lambda}{U(T_f - T_p)}. \quad (20)$$

The surface temperature at the feed side is given by the equations below, deriving from Eqs. (13), (14) and (15) [72]:

$$T_{fm} = T_f - \frac{(T_f - T_p) \frac{1}{h_f}}{\frac{1}{h_v + \frac{k_m}{\delta}} + \frac{1}{h_p} + \frac{1}{h_f}}, \quad (21)$$

in which:

$$h_v = \frac{J\lambda}{T_{fm} - T_{pm}}. \quad (22)$$

Equation (21) is applicable in the most general case. On the other hand, if the difference $T_{fm} - T_{pm}$ is less than 10 °C in a MD unit and for dilute solutions, Eq. (23) defines the pure water flux quite accurately:

$$N = C \frac{dP}{dT} \Big|_{T_m} (T_{fm} - T_{pm}). \quad (23)$$

This relation is based on the statement that for limited temperature ranges between feed and permeate, the following equation is valid:

$$\frac{(p_{fm} - p_{pm})}{(T_{fm} - T_{pm})} \Big|_{T_m} = \frac{dP}{dT} \Big|_{T_m}, \quad (24)$$

where, according to the model of Clausius-Clapeyron, $\frac{dP}{dT} \Big|_{T_m} = \frac{P\lambda MW_s}{RT^2} \Big|_{T_m}$ whilst pressure can be evaluated from the Antoine equation as $P = \exp\left(23.238 - \frac{3841}{T_m - 45}\right)$.

Considering that feed and permeate produce the same temperature polarization, T_m can be defined as:

$$T_m = \frac{T_f + T_p}{2}. \quad (25)$$

Equations (14) and (23) allows to write the total heat transfer across the membrane as follows:

$$Q_m = \left(\frac{k_m}{\delta} + C \frac{dP}{dT} \Big|_{T_m} \lambda \right) (T_{fm} - T_{pm}). \quad (26)$$

Q_m can be also expressed as:

$$Q_m = H(T_{fm} - T_{pm}), \quad (27)$$

where H is the effective heat transfer coefficient of the membrane.

From Eqs. (13), (15) and (27):

$$(T_{fm} - T_{pm}) = (T_f - T_p) \left(1 + \frac{H}{h_{fm}} + \frac{H}{h_{pm}} \right). \quad (28)$$

From Eqs. (23) and (28), and substituting the overall film heat transfer coefficient $h = \frac{1}{\left(\frac{1}{h_{fm}} + \frac{1}{h_{pm}}\right)}$ gives:

$$N = C \frac{dP}{dT} \Big|_{T_m} \frac{(T_f - T_p)}{\left(1 + \frac{H}{h}\right)}. \quad (29)$$

Substituting in the previous equation $H = \frac{k_m}{\delta} + C \frac{dP}{dT} \Big|_{T_m} \lambda$ from Eq. (27) and rearranging, the relation below can be obtained:

$$\frac{T_f - T_p}{N\lambda} = \frac{1}{\frac{dP}{dT} \Big|_{T_m}} \frac{1}{C\lambda} \left(1 + \frac{k_m}{\delta} \right) + \frac{1}{h}. \quad (30)$$

The only unknowns of Eq. (30) are h and C . Plotting $\frac{T_f - T_p}{N\lambda}$ vs. $\frac{1}{\frac{dP}{dT} \Big|_{T_m}}$ yields $\frac{1}{h}$ as intercept and $\frac{1}{C\lambda} \left(1 + \frac{k_m}{\delta} \right)$ as slope from which the value of C can be determined.

3.2 AGMD

In the AGMD configuration, the mass transport across the feed bulk and the membrane surface on the permeate side can be written using the same equations obtained for studying DCMD. However, the air gap flux differs from that exhibited on the permeate side in the DCMD configuration. The flux N can be written as follows:

$$N = \frac{P_{pm} - P_{cf}}{R_{ag}}, \quad (31)$$

where P_{cf} is the water vapor pressure at the condensing film while R_{ag} is the mass transport resistance in the air gap. The latter can be defined as:

$$R_{ag} = \left[\frac{\delta_a P_{ln,g} RT_{ln,g}}{\varepsilon D P M W_s} \right], \quad (32)$$

in which δ_a is the air gap width, D the water vapor coefficient, and P_{ln} and T_{ln} the logarithmic mean pressure

and temperature within the air gap, respectively. The total resistance to mass transfer R_{AGMD} is then:

$$R_{AGMD} = R_m + R_{ag}, \quad (33)$$

where R_m can be calculated by Eq. (8), (9) or (10). The total flux in AGMD is defined by the following equation:

$$N = \frac{P_{fm} - P_{cf}}{R_{AGMD}}. \quad (34)$$

Regarding the heat transfer, Eq. (14) is suitable to describe the thermal flux across the membrane in AGMD, too. The other relevant heat transports associated to this configuration are: the heat transfer in the air gap (Q_{ag}), the heat transfer across the falling film (Q_{cf}), the heat transfer across the condensing plate (Q_{cp}) and the heat transfer for the coolant channel (Q_c). They are listed below:

$$Q_{ag} = \frac{K_{ag}}{\delta_a} (T_{pm} - T_{cf}) + N\lambda, \quad (35)$$

$$Q_{cf} = \frac{K_{cf}}{\delta_{cf}} (T_{cf} - T_{cw}), \quad (36)$$

$$Q_{cp} = \frac{K_{cp}}{\delta_{cp}} (T_{cw} - T_{cc}), \quad (37)$$

$$Q_c = h_c (T_{cc} - T_c), \quad (38)$$

where K_{ag} = thermal conductivity of the air/water mixture in the air gap; T_{cf} = surface temperature of the condensing film; K_{cf} = thermal conductivity of condensed water; δ_{cf} = thickness of the condensed film; T_{cw} = interface temperature between the condensed film and the condensing plate; K_{cp} = thermal conductivity of the condensing plate; δ_{cp} = thickness of the condensing plate; T_{cc} = interface temperature between the condensing plate and the cold fluid; h_c = convective heat transfer coefficient; T_c = temperature of the cooling fluid.

3.3 SGMD

Equations (12), (13), (14) and (15) (used to describe the DCMD configuration) can be applied to the development of mass and heat transport models for SGMD [73]. In effect, except that a sweeping gas flows on the permeate side instead of cold water, the two processes are very similar. However, it should be noted that the condenser, the presence of which is inevitable in this configuration, can involve significant costs.

3.4 VMD

Since in VMD the cold permeate is replaced by vacuum, the flux can be calculated as:

$$N = \frac{P_f - P_v}{R_f + R_m}, \quad (39)$$

where P_v is the vacuum pressure. Because of the high velocity of the process, the conductive heat transport through the membrane can be neglected in the heat balance as shown below:

$$Q = N\lambda = h_f(T_f - T_{fm}). \quad (40)$$

As well as for SGMD, the costs associated to the VMD condenser can affect the economic feasibility of the entire process.

4 Concentration polarization coefficient

The concentration polarization coefficient (ζ) considers the accumulation of solute on the membrane surface. It is defined as follows:

$$\zeta = \frac{c_{fm}}{c_f}, \quad (41)$$

with c_{fm} the salt concentration at the hot membrane surface, and c_{fb} the salt concentration in the feed bulk solution. If $\zeta \rightarrow 1$, then $c_{fm} \approx c_f$ and the concentration polarization phenomenon becomes negligible. In the case of complete rejection of the solute, as one would expect from hydrophobic membranes, the following equation is physically consistent [67]:

$$\zeta = \exp\left(\frac{J}{\rho K_c}\right), \quad (42)$$

where ρ is the solution density and K_c is the solute mass transfer coefficient. Concentration polarization occurs only at higher feed concentrations. Overall, it can be said that the impact of the concentration polarization phenomenon is very limited in MD/MCr operations and can be neglected most of the time.

5 Temperature polarization coefficient

The temperature polarization coefficient (TPC) gives account for the thermal efficiency of the process that can be significantly reduced by decreasing membrane thermal conductivity as well as with an improvement in fluid dynamics inside the membrane module. TPC correlates the difference of temperature at membrane surfaces to the corresponding difference in the bulk:

$$TPC = \frac{T_{fm} - T_{pm}}{T_f - T_p}. \quad (43)$$

The value of TPC ranges from 0 to 1, being the latter associated with a thermally efficient process. The more TPC approaches 0, the more the driving force of the

membrane distillation reduces, which is highly undesirable [68]. The value of TPC increases with higher Reynolds numbers since high flow speeds reduce the resistance to the mass transfer of the feed side boundary layer and increase the heat transfer from the bulk to the membrane surface. On the other hand, TPC reduces at higher feed inlet temperatures. This is because of the decrease of the membrane surface temperature on the feed side, owing to the cooling effect induced by fast evaporation, and the increase of the membrane surface temperature on the permeate side caused by the transmembrane heat flux. Actually, even though the Reynolds number of the feed stream increases at high feed inlet temperatures, the increased heat transfer drives the value of TPC down. There is another parameter affecting TPC : feed concentration. Viscosity and density increase as a result of raising feed concentration. While the increased solution viscosity slows down the vapor diffusion and the heat transport from the bulk to the feed membrane surface, viscosity and

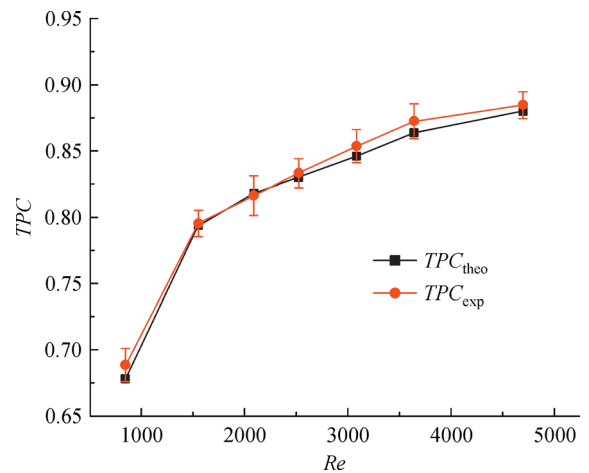


Fig. 4 Theoretical and experimental TPC as a function of Reynolds number. Reprinted with permission from ref. [31], copyright 2013, Elsevier.

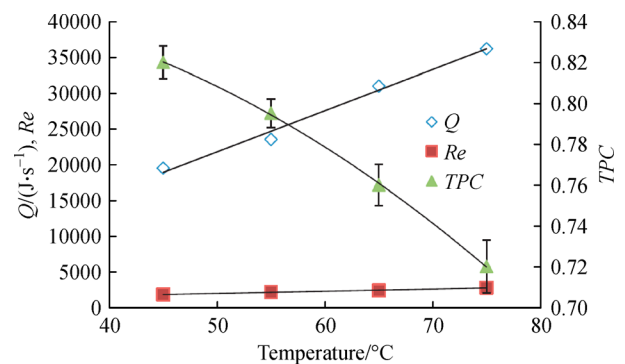


Fig. 5 Total heat flux, Reynolds number and TPC as a function of feed inlet temperatures. Reprinted with permission from ref. [31], copyright 2013, Elsevier.

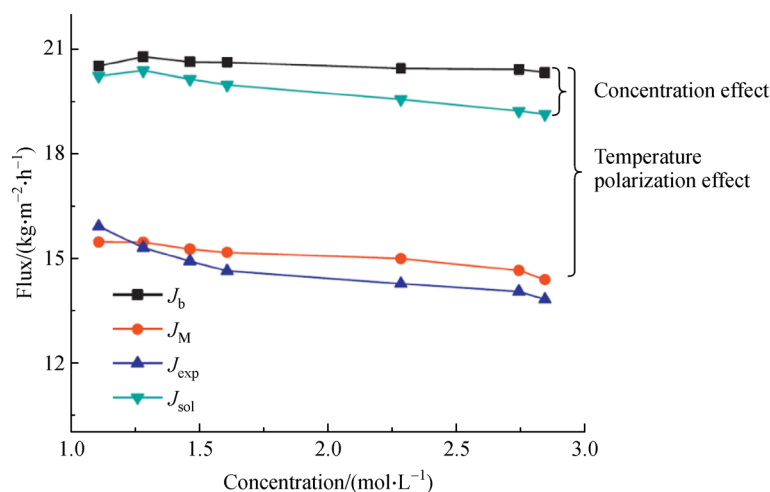


Fig. 6 Dependence of transmembrane flux, calculated on the basis of different considerations, on feed solution concentration. J_b , J_M , J_{exp} and J_{sol} represent the flux calculated using bulk temperatures, membrane surface temperatures, bulk temperatures combined with solution concentration effects and experimental flux, respectively. Reprinted with permission from ref. [31], copyright 2013, Elsevier.

density jointly contribute to the reduction of the Reynolds number of the feed stream. It follows that both these phenomena decrease the value of TPC . The impact of Reynolds number, feed inlet temperature and feed concentration on temperature polarization can be seen from Figs. 4, 5 and 6, respectively. They are all referred to the same experiments performed by using temperature sensors, positioned inside the membrane module, that allowed to measure the bulk and surface temperatures in a DCMD system in different operating conditions [31]. According to Fig. 4, both theoretical and experimental data confirm that TPC increases at higher Reynolds numbers. Figure 5 highlights the fact that an increase in feed inlet temperature corresponds to higher values of total heat flux transported across the membrane and Reynolds number, while the TPC is significantly reduced. Finally, Fig. 6 presents the quantitative role of solution concentration in flux reduction. In addition to including the experimental flux (J_{exp}), it also shows the trends of transmembrane fluxes calculated on the basis of different assumptions as J_b , J_M and J_{sol} are evaluated considering the bulk temperatures, the membrane temperatures and both bulk temperatures and solution concentration effects, respectively. As one can notice from the figure, the temperature polarization effect always prevails over the concentration effect in reducing the transmembrane flux, at increasing feed concentrations.

6 Optimization of module length

The ITM (Italy) and INC (South Korea) research groups were the first to address the issue of optimization of module length for hollow fiber membranes in DCMD

rather than flat sheet membranes. The optimum module length ($L_{m,opt}$) for hollow fiber membranes in DCMD has been estimated by means of cost analysis by Ali et al. [74]. Cost analysis is based on the evaluation of total costs (TC), subdivided into operational costs (OP) and fixed costs (FC) so that the value of $L_{m,opt}$ can be derived by the minimization of TC . OP comprise steam, electricity, chemical and membrane replacement costs, while the main cost items of FC are the heat exchanger area and the membrane module. The parameters affecting the value of $L_{m,opt}$ are the feed inlet temperature, membrane thickness and recovery factor. It has been observed that TC decreases, or equivalently the module length becomes optimal, in the following circumstances: at higher feed inlet temperatures (associated with increased thermal efficiencies, high fluxes and decreased heat exchanger areas), with thicker membranes (in which conduction losses are reduced and a larger portion of the fiber contributes to the transmembrane flux), and at higher recovery factors (implying a diminished feed inlet volume and a reduced thermal energy consumption). According to another definition, $L_{m,opt}$ can be defined as the module length that minimizes the SEC function, defined as the ratio between the heat duty of the MD process and the productivity (the product of the average flux and the corresponding membrane area) [75]. It was found that the value of $L_{m,opt}$ for a generic DCMD membrane strongly depends on feed inlet temperature, solution concentration and membrane thickness. The computer simulation has allowed to observe that when F/P (i.e., the reciprocal of the recovery factor) is fixed, $L_{m,opt}$ increases with feed inlet temperature while decreasing at higher F/P ratios, associated with reduced productivity and heat duty. The

evaluation of the effect of feed salinity showed that $L_{m,opt}$ increases by decreasing solution concentration for any given F/P ratio because of the reduction of the driving force at high salt concentrations. The simulation has also allowed to verify that $L_{m,opt}$ increases at higher values of membrane thickness, less energy dispersive. As a result of the optimization work, a 48 cm long and 20 μm thick membrane working with 8% (w/w) solution concentration has been proposed as example of optimized membrane. In agreement with these results, a hollow fiber membrane with a similar length (40 cm), produced by Econity, has been adopted in the SWRO-MD pilot plant designed in the framework of the GMVP project in Busan (South Korea).

7 Exergy analysis

As much as the energetic analysis is useful in determining the energetic requirements of the considered system, it is the exergy analysis that allows to measure the effective energy use, to identify the critical energetic losses and to fix them [76–79]. The total energy of a system can be divided in exergy and anergy [80], the first one corresponding to a form of energy that can be converted through reversible transformations from one form to another, while the second one being seen as the dissipative part of energy that degrades as heat to the surrounding environment. In other words, exergy represents the maximum work achievable by a system that undergoes a reversible transformation from a non-equilibrium to a state in equilibrium with the environment, taken as a reference state [26,78]. For a fluid system whose governing intensive parameters are temperature, pressure and composition, exergy (E_X) is described by the following equation in which these three contributions are clearly identifiable:

$$E_X = G \left[c_p(T - T_0) - c_p T_0 \ln \left(\frac{T}{T_0} \right) + \left(\frac{P - P_0}{\rho} \right) - N_s R T_0 \ln x_1 \right] \\ = E_X^T + E_X^P + E_X^c, \quad (44)$$

where G = mass flow, T_0 = reference temperature, P_0 = reference pressure, c_p = specific heat of the solution, N_s = moles of solvents per unit weight of solution

$$= \frac{1000 - \sum \frac{c_i}{\rho}}{MW_s}, \quad c_i = \text{weight concentration of the } i\text{-th component per liter of solution, } x_i = \frac{N_s}{N_s + \sum \frac{\beta_i c_i}{\rho MW_i}},$$

β_i = number of particles generated by the dissociation of the i -th component in the solution, MW_i = molecular weight of the i -th component.

The contribution of concentration to exergy (E_X^c) is calculated assuming pure water at T_0 and P_0 as reference

state. Each transformation corresponds to a variation of exergy as follows:

$$\Delta E_X = -T_0 R_S + W_U + W'_U \\ = \sum_i E_{X,i} - \sum_k E_{X,k}, \quad (45a)$$

and

$$T_0 R_S = W_U + W'_U - \Delta E_X, \quad (45b)$$

where R_S = rate of production of entropy, $T_0 R_S$ = total energy destroyed and transformed irreversibly in entropy [$\text{kJ} \cdot \text{h}^{-1}$] (as illustrated by Eq. (45b)), W_U = electric exergy supplied to the system [$\text{kJ} \cdot \text{h}^{-1}$], W'_U = thermal exergy supplied to the system [$\text{kJ} \cdot \text{h}^{-1}$], i = inlet stream, k = outlet stream.

W_U and W'_U are often operatively determinable so that the term $T_0 R_S$ could be derived by the equations above. The exergetic efficiency is typically defined as:

$$\varepsilon_X = \frac{E_{X,output}}{E_{X,input}}, \quad (46)$$

where $E_{X,output}$ represents the exergy exiting the system and $E_{X,input}$ represents the value of exergy entering the system. The term $T_0 R_S$ of Eqs. (45a) and (45b) is the energy generation, or equivalently the exergy consumption. It is expressed in $\text{kJ} \cdot \text{h}^{-1}$ and corresponds to the product of the generated entropy and the reference temperature [81].

The exergy content of a stream is determinable if flow rate, temperature, pressure and composition are known while the exergy of a process can be calculated from values of processed flow rates, temperature and pressure of the operation, efficiency of the various equipment (if any), electric energy consumption (if any) and thermal energy consumption (if any). The application of the exergetic analysis to MD/MC_r units showed that, because of the low operating pressures, the electric energy consumption term is considerably smaller than that of pressure-driven membrane processes while the thermal energy requirement of the feed inlet stream is not negligible [77]. Such a heat load increases the irreversible production of entropy and inevitably the global energy demand [77]. On the other hand, when the required thermal energy is available in the plant through the use of heat recovery systems, the MD/MC_r applications can compete with other desalination processes because of their higher exergetic efficiency [82]. In general, the lower the operative temperature of the feed stream, the less its thermal energy requirement is and the values of W'_U and $E_{X,input}$ accordingly. The exergetic analysis is particularly effective in comparing different integrated membrane systems. It has been used to determine the best position of a MD/MC_r unit for a simple flow sheet taken as a reference [77]. Moreover, this

calculation approach allows to find alternative process designs that result in a reduction of entropic losses (for example the replacement of expansion valves with energy recovery devices such as Pelton wheel and pressure exchanger system- or the availability of thermal energy in the plant) [76,78]. Exergy analysis of an integrated membrane desalination system with RO, MD and RED (Reverse ElectroDialysis) units was carried out by Tufa et al. [83], too. They proved that the highest exergy efficiency (53%) can be achieved when working at the lowest water recovery factor (75%) and temperature (40 °C). The specific energy consumptions associated with the analyzed configuration was $3.5 \text{ kWh} \cdot \text{m}^{-3}$ and, in agreement with [78], this value can be reduced in case of the availability of free thermal supply sources.

8 Membrane materials and thermal conductivity

The main barrier to the spread of MD/MCr technology for water desalination is due to the lack of high-performing membranes that would completely replace RO [32]. MD/MCr membranes are required to be porous, hydrophobic, chemically resistant and thermally stable. However, there is no doubt that the thermal conductivity of a membrane material is one of the critical parameters as it influences mass and heat transfer as well as membrane porosity and thickness. This is because thermal conduction is considered as a heat loss mechanism, as no corresponding mass transfer takes place. In principle, the membrane surface should be made of material with small thermal conductivity; however, the thermal conductivities of most hydrophobic polymers are close to each other. For example, the thermal conductivity of PVDF, PTFE and PP are 0.21–0.37, 0.25–0.27 and 0.11–0.16 $\text{W} \cdot \text{m}^{-1} \cdot \text{K}^{-1}$, respectively. To improve the performance of MD membranes, one possibility is to consider the use of microporous composite membrane, with a top hydrophobic thin layer responsible for the mass transport, and a hydrophilic sub-layer able to reduce the conductive heat loss through the whole membrane matrix. An example can be found in [84], where a low thermally conductive tetra-fluoroethylene/2,2,4-trifluoro-5-tri-fluoromethoxy-1,3-dioxol (HYFLON AD 60) nanofilm was suspended onto a PES honeycomb texture for the fabrication of a nanostructured membrane. The membrane tested in MD operation with $5 \text{ mmol} \cdot \text{L}^{-1}$ salty solutions exhibited better performance (in terms of flux and thermal efficiency) when compared with other home-made and commercial membranes. An average water flux of $51 \text{ L} \cdot \text{m}^{-2} \cdot \text{h}^{-1}$ versus a thermal efficiency of 70.2% was measured for the composite nanostructured membrane, whereas fluxes less than $5 \text{ L} \cdot \text{m}^{-2} \cdot \text{h}^{-1}$ and thermal efficiency not superior to 35% were estimated for commercial membranes in PP traditionally used in DCMD

operations [26]. Other membranes processed at much higher feed temperature showed a thermal efficiency ranging from 55% to 80% approximately, but an average flux much lower (less than $13 \text{ L} \cdot \text{m}^{-2} \cdot \text{h}^{-1}$) [85].

Recently some new materials have received attention for improving wetting resistance, thermal stability, chemical resistance and mechanical strength of MD membranes; sometimes, however, neglecting the thermal conductivity of the material. One of these is graphene. The latter is an interesting material with several applications due to its very high thermal stability and electric conductivity, high mechanical stiffness, low permeability to water, and is low cost. In addition to its use in various fields (foldable electronics, biological engineering, composite materials, energy storage), recent researches have shown that, due to its high aspect ratio and high specific surface area, graphene is an ideal filler that could promote better interaction with the host polymer [86]. Water and vapor molecules cannot penetrate via pure graphene pore due to its unique nature [87]. Graphene is particularly attractive for MD application due to its hydrophobic nature, selective sorption of water vapors, and anti-fouling properties [87–89]. Moreover, the incorporation of graphene provides additional properties to the composite membrane such as added roughness and hydrophobicity that leads to robust and highly efficient MD membranes.

Graphene membrane with thickness near 1 nm has shown high mechanical strength and excellent selectivity toward various gases [57]. Thanks to these features, it is possible to reduce the thickness of the graphene-based membranes and to apply them in desalination applications including MD. The drawback of graphene is its very high thermal conductivity ($\sim 5000 \text{ W} \cdot \text{m}^{-1} \cdot \text{K}^{-1}$) in the in-plane direction at 300 K for graphene [90] and $\sim 2000 \text{ W} \cdot \text{m}^{-1} \cdot \text{K}^{-1}$ for graphite [91]), as they could originate significant polarization events. Therefore, the use of graphene in thermally driven operations could be in principle unsuitable. Nevertheless, various applications of graphene membranes in MD can be found in literature [86,92–95].

Other two-dimensional (2D) materials of atomic thickness represent the next generation membrane materials with extraordinarily high permeability. Examples can be found in the transition metal dichalcogenide monolayers recently introduced in PVDF-based membranes to enhance the performance of membrane distillation and membrane crystallization processes [96,97]. In particular, Bi_2Se_3 crystals [97] and Bi_2Te_3 flakes [98] were incorporated in PVDF based membranes and tested in MCr the crystallization of NaCl. Topological insulators such as Bi_2Te_3 and Bi_2Se_3 , also known as “graphene like materials”, are characterized by excellent surface electric conductivity, comparable to that of graphene. However, compared to the latter, they have a very low thermal conductivity ($0.4 \text{ W} \cdot \text{m}^{-1} \cdot \text{K}^{-1}$ for Bi_2Se_3 and $1.6 \text{ W} \cdot \text{m}^{-1} \cdot \text{K}^{-1}$ for Bi_2Te_3)

and they can be produced by relatively inexpensive processes. All this makes them particularly suitable for MD and MCr processes.

9 Wetting and fouling in MD/MCr systems

Wetting is a common problem in MD applications. It consists in a liquid contacting with a solid membrane through intermolecular interactions [99]. When a porous membrane gets wet, the liquid phase penetrates the pores because the transmembrane pressure exceeds the LEP_w (discussed in Sec. 2.1). There are two types of wetting: partial pore wetting and complete wetting. While the former is associated with vapor flux decline (due to the blockage of some pores of the membrane), the second implies a steep rise in flux due to the direct liquid passage across the membrane pores [69,100,101]. As a result of wetting, either partial or complete, salt rejection decreases and the distillate electric conductivity increases [8,69,102]. It is interesting to note that wetting phenomenon typically affects MD operations based on the phase transition from liquid to vapor, whereas it is absent in RO, as in the other pressure-driven membrane processes in which the liquid is forced to penetrate through the membrane pores [103]. Anyway, the performance of both membrane operations is negatively influenced by the fouling problem even though membrane fouling in MD is thought to be less severe than in conventional RO [104]. As earlier described in section 2.4, fouling is the accumulation of unwanted materials on the surface or inside the pores of a membrane and has a detrimental impact on the overall performance of MD operations [40]. Scaling at the membrane surface is the most common form of fouling in MD desalination applications [22]. It usually stimulates the onset of wetting [34]. Key factors that influence wetting and fouling in MD are the following: (a) membrane surface properties (wettability, roughness, surface tension, surface charge, pore size, and surface functional groups), (b) fluid dynamics (flow velocity, motion direction, temperature, local hydrostatic pressure gradient) and (c) feed characteristics (mole fraction, diffusivity, nature of foulants, charge, pH) [34]. A significant research effort has recently been conducted with the aim of preventing wetting and fouling, with a particular attention to membranes with special wettability among which the superhydrophobic, omniphobic and Janus membranes deserve to be considered [34]. The superhydrophobic membranes are characterized by contact angles greater than 150° allowing them to improve flux and long-term MD operation [106]. The superhydrophobic glass MD membrane developed by Ma et al. consisted in nano-spiked microchannels on the membrane surface allowing to increase the contact angle up to 160° [107]. Razmjou et al. increased the surface roughness of a PVDF membrane by incorporating fluorinated TiO_2 nanoparticles that generated hierarchical

structures [106]. Su et al. fabricated a robust superhydrophobic membrane for MD by combining electro-co-spinning/spraying with chemical vapor welding [108]. The produced membranes were tested using sodium chloride and gypsum as feed impurities and revealed to be very effective in mitigating mineral scaling. Although superhydrophobic membranes lead to improved permeability and wetting resistance, they are affected by organic fouling in presence of oil emulsions in the feed water, as well as the hydrophobic membranes [35]. The main feature of omniphobic membrane surfaces is their ability to repel liquids with a broad spectrum of surface tensions including mineral oils, decane and ethanol so as to prevent the occurrence of wetting and fouling when low surface tension feeds are treated in MD. The first omniphobic MD membrane is ascribed to Lin et al. [109]. By coating silica nanoparticles on glass membranes and subsequent fluorination, they were able to create air-trapping reentrant structures which displayed high contact angles toward various low surface tension liquids. A similar approach based on the obtaining morphologies that generate repellency was proposed by Lu et al. [110]. They developed an omniphobic PVDF membrane by silica nano-particle deposition and coating with Teflon and tested it using a feed solution containing $0.6 \text{ mmol} \cdot \text{L}^{-1}$ of sodium dodecyl sulfate giving proof of stable performance in VMD. On the other hand, Woo et al. [111] made electrospun nanofibrous membranes undergo CF_4 plasma treatment that induced the reduction in surface energy by the growth of CF_2 - CF_2 and CF_3 interactions. After a 15 min CF_4 plasma treatment, the average contact angle improved from 133° to 160° . Despite their contribution in providing fouling and wetting resistance with low surface tension contaminants, omniphobic membranes are difficult to fabricate and could potentially poison the waters in contact with them, since they contain toxic compounds [35]. Janus membranes are characterized by opposing wettability at each side [112] inherently due to the different morphology, surface charge and material component. Khayet et al. [49] proposed a MD membrane with a hydrophobic layer on a hydrophilic layer. The porous membrane was prepared by phase inversion using a polymer dope solution containing hydrophobic fluorinated surface-modifying macromolecules. In this membrane, the hydrophobic thin top-layer decreases the resistance to mass flux while the thicker low-conductive hydrophilic sub-layer reduces the heat loss. In contrast, Chen et al. [113] succeeded in creating a composite Janus membrane, with a hydrophilic top-layer and hydrophobic substrate displaying excellent anti-wetting performance. More specifically, the dense hydrophilic layer, highly resistant to surfactant-containing saline water, was obtained by layer-by-layer assembling cationic polyethyleneimine and anionic poly (sodium 4-styrenesulfonate) polyelectrolytes on a PVDF hydrophobic substrate. Even if Janus membranes can contribute to improve flux and wetting resistance in MD,

they present the following limitations: it is difficult to fabricate special wettability coatings on hollow fiber membranes at a large scale [34] and there is not a clear understanding of stimuli-responsive functionalities of Janus membranes [114].

Experimental observations related to MCr tests involving PP membranes or Hyflon AD/PVDF composite membranes, and LiCl as solute, are reported hereafter. They are an example of how some of the abovementioned parameters are crucial in understanding the occurrence of wetting in MD/MCr operations. Given that the solubility of LiCl is very high at 25 °C [99,100], $\sim 19.6 \text{ mol}\cdot\text{L}^{-1}$, and increases yet further with temperature, it cannot be crystallized at the operating conditions of DCMD because the osmotic effects overcome the thermal effect and a negative flux occurs. As shown in Table 5, LiCl solubility is quite remarkable if compared to that of the other alkali metal chlorides (MCl). From crystallization tests with commercial PP membrane modules in DCMD it has been found that the maximum achievable concentration for a LiCl solution starting from $6 \text{ mol}\cdot\text{L}^{-1}$ cannot go beyond $7 \text{ mol}\cdot\text{L}^{-1}$ at feed inlet temperature of 52 °C [115]. This is because when the concentration increases at feed side, the vapor pressure of feed solutions reduces, the osmotic pressure increases significantly and the transmembrane flux approaches zero, preventing the supersaturation from being achieved. To overcome these difficulties VMD has been employed using the same PP membranes with good results [115]. Differently from DCMD, VMD with PP membranes allows to reach supersaturation of LiCl. The ease of VMD in concentrating the salts in the feed is attributable to the absence of temperature polarization and cold stream on the permeate side due to the direct withdraw of water vapor from the feed side by means of a vacuum pump. Nevertheless, further experiments in VMD involving Hyflon AD/PVDF as membrane material in place of PP, have revealed that Hyflon AD/PVDF induces complete wetting, with no salt precipitation. The chemical interaction solute-membrane may play a role in explaining the different behavior displayed by PP and Hyflon AD/PVDF in the crystallization of LiCl in VMD. Hyflon AD and PVDF are much more electronegative than PP. Electronegativity, as known, is a measure of how easily an atom attracts electrons. According to the Pauling scale, fluorine is the most electronegative element, with an assigned value of 3.98, while the electronegativity of carbon and hydrogen is 2.55 and 2.20. When there are no polar bonds in a molecule, there is no permanent charge difference between one part of the molecule and another. For example, the C–C and C–H bonds in hydrocarbon molecules are not significantly polar and hydrocarbon polymers like PP are non-polar too [116]. Since the polarity of molecules affects the structure of the polymer and the attraction of polar molecules, one could conclude that Hyflon AD and PVDF tend to react chemically with ions dissolved in water, as opposed to PP. Nevertheless, PVDF and composite Hyflon

AD/PVDF membranes have been successfully employed for NaCl crystallization at supersaturated concentrations [117]. Experimental data, supported by computational simulations, showed that there are no significant differences in the nucleation and growth of NaCl crystals in MCr, conducted using PP or PVDF membranes [117]. However, it is common knowledge that PVDF displays excellent resistance to halogens, whereas is not completely resistant to alkali metals [118] and LiCl is often employed as pore forming in PVDF matrices because of its chemical reactivity with F [119,120]. It follows that when the alkaline concentration is particularly high in the proximity of the membrane surface, as expected in VMD for a very soluble salt like LiCl, the interaction metal-PVDF becomes much more prominent and gives rise to the wetting phenomenon. When the concentration of the dissolved LiCl increases in VMD, the number of cations (Li^+) interacting with the PVDF membrane surface increases too. Since PVDF is thought to be an electron donor macromolecule in the presence of LiCl, it is reasonable to hypothesize the formation of changeable networks between PVDF and LiCl on the surface of the membrane, at the operating temperatures of MCr [119,120]. It may be also presumed that the reason why such chemical behavior does not occur with single salt solutions of NaCl, at the same operative conditions, is that the strength of the chemical bond between Li and fluorinated compounds is far above the one exhibited by Na^+ in presence of anions containing F [121]. Furthermore, LiCl vacuum membrane crystallization (VMCr) experiments with ceramic membranes support the hypothesis that fluopolymeric membrane materials prevent LiCl crystallization. The complexity of the phenomena involved induce to explore the role played by materials and operating conditions in crystallization. In further studies, it could be interesting to quantify the level of reactivity of different PVDF materials and verify the crystallization behavior of LiCl at different Reynolds. Furthermore, performing MCr experiments with other chlorides can certainly enrich knowledge on crystallization of alkali metals.

Table 5 Solubility of alkali metal chlorides

| M (Alkali Metal) | Solubility of MCl/(mol·L ⁻¹) |
|------------------|--|
| Li | 19.6 |
| Na | 6.2 |
| K | 4.8 |
| Rb | 7.5 |
| Cs | 11.0 |

10 Conclusions

MD is a promising thermally driven separation process that is gaining an increasing attention worldwide in the

framework of water desalination technologies. The principle of operation of MD is very similar to MCr, a process that combines MD with crystallization and can significantly contribute to the recovery of valuable crystals from supersaturated solutions. MD works at lower operating temperatures than MSF and MED, typically below 70 °C feed side and 50 °C permeate side and lower operating pressures than RO, usually up to 1 bar, providing a 100% theoretical rejection of nonvolatile solutes in the almost complete absence of concentration polarization phenomena. Nevertheless, it can result in temperature polarization and membrane pore wetting. The former is inevitable and can be mitigated mainly by changing the fluid dynamics of the system while the latter can primarily be reduced or completely prevented by choosing appropriate fluid dynamics conditions and suitable membrane materials, as is evident from experimental observations involving LiCl with composite Hyflon AD/PVDF membranes. In this respect, the occurrence of wetting in crystallization tests with Hyflon AD/PVDF membranes but not in presence of PP or ceramic membranes, all performed in VMCr, can presumably be attributed to the chemical interaction between the positively charged Li and fluoropolymers, acting as electron donor macromolecules.

Each MD configuration has its own specific material and energy balance equations, which are the starting point for the evaluation of optimized parameters. The optimum module length is one of the most studied and, according to Ali et al. [75], it can be esteemed that a good reference length for hollow fibers employed in DCMD applications is 48 cm.

The application of the exergetic analysis to MD/MCr systems shows that the electric energy consumption term is somewhat small if compared to that of pressure-driven membrane processes such as RO but the thermal energy requirement can be very high. However, the impact of the thermal energy term for a generic MD/MCr process can be mitigated by the use of heat recovery systems employing heat available in the plant that would otherwise be wasted.

While MD/MCr applications make an important contribution to salt water management by enabling the production of fresh water and the recovery of precious salts, there is still a long way to go before these technologies can become widespread. Further research efforts should be addressed to the study of optimized couplings of membrane configurations (which have a direct effect on fluid dynamics) and membrane materials (whose physicochemical properties can inevitably impact on the transmembrane flux and occurrence of wetting). MD performance confirms the need for a customized hardware, i.e., high porosity hydrophobic membranes with appropriate thickness and made by low-heat conductive polymers in order to reduce the amount of waste energy. New amorphous perfluoropolymers, mixed matrix and ceramic materials are becoming available. Moreover, clear protocols and comparison indexes for the choice of the best

materials and operative conditions, accurate modeling for an easy scale-up or scale-down, and significant multi-disciplinary research efforts are needed and might contribute to the development of the technology.

References

1. Eckhardt N A, Cominelli E, Galbiati M, Tonelli C. The future of science: food and water for life. *Plant Cell*, 2009, 21(2): 368–372
2. Boretti A, Rosa L. Reassessing the projections of the world water development report. *NPJ Clean Water*, 2019, 2(1): 1–6
3. Shannon M A, Bohn P W, Elimelech M, Georgiadis J G, Mariñas B J, Mayers A M. Science and technology for water purification in the coming decades. *Nature*, 2009, 452(7185): 301–310
4. Pinto F S, Marques R C. Desalination projects economic feasibility: a standardization of cost determinants. *Renewable & Sustainable Energy Reviews*, 2017, 78: 904–915
5. GWI and IDA. IDA Water Security Handbook 2018–2019. Oxford (United Kingdom): Media Analytics Ltd., 2018, 4–28
6. Kesieme U K, Milne N, Aral H, Cheng C Y, Duke M. Economic analysis of desalination technologies in the context of carbon pricing, and opportunities for membrane distillation. *Desalination*, 2013, 323: 66–74
7. Ali A, Tufa R A, Macedonio F, Curcio E, Drioli E. Membrane technology in renewable-energy-driven desalination. *Renewable & Sustainable Energy Reviews*, 2018, 81: 1–21
8. Gryta M. Capillary polypropylene membranes for membrane distillation. *Fibers (Basel, Switzerland)*, 2019, 7(1): 1
9. Curcio E, Criscuoli A, Drioli E. Membrane crystallizers. *Industrial & Engineering Chemistry Research*, 2001, 40(12): 2679–2684
10. Drioli E, Criscuoli A, Curcio E. Membrane contactors: Fundamentals, Applications and Potentialities. 1st ed. Amsterdam: Elsevier, 2006, 24
11. Macedonio F, Drioli E. Special issue of desalination journal on “membrane engineering for desalination in the mining and extraction industry”. *Desalination*, 2018, 440: 1
12. Quinst-Jensen C A, Macedonio F, Drioli E. Integrated membrane desalination systems with membrane crystallization units for resource recovery: a new approach for Mining from the sea. *Crystals*, 2016, 6(4): 36
13. Chabanon E, Mangin D, Charcosset C. Membranes and crystallization processes: state of the art and prospects. *Journal of Membrane Science*, 2016, 509: 57–67
14. Macedonio F, Quinst-Jensen C A, Al-Harbi O, Alromaih H, Al-Jlil S A, Al Shabouna F, Drioli E. Thermodynamic modeling of brine and its use in membrane crystallizer. *Desalination*, 2013, 323: 83–92
15. Biniáz P, Torabi Ardekani N, Makarem M A, Rahimpour M R. Water and wastewater treatment systems by novel integrated membrane distillation (MD). *ChemEngineering*, 2019, 3(1): 8
16. Zaragoza G, Andrés-Mañas J A, Ruiz-Aguirre A. Commercial scale membrane distillation for solar desalination. *NPJ Clean Water*, 2018, 1(1): 1–6
17. Guillén-Burrieza E, Blanco J, Zaragoza G, Alarcón D C, Palenzuela P, Ibarra M, Gernjak W. Experimental analysis of an

- air gap membrane distillation solar desalination pilot system. *Journal of Membrane Science*, 2011, 379(1–2): 386–396
18. Koschikowski J, Wiegand M, Rommel M, Ortin V S, Suarez B P, Rodríguez J R. Experimental investigations on solar driven stand-alone membrane distillation systems for remote areas. *Desalination*, 2009, 248(1–3): 125–131
 19. Schwantes R, Bauer L, Chavan K, Dücker D, Felsmann C, Pfafferoth J. Air gap membrane distillation for hypersaline brine concentration: Operational analysis of a full-scale module—New strategies for wetting mitigation. *Desalination*, 2018, 444: 13–25
 20. Ruiz-Aguirre A, Andrés-Mañas J A, Fernández-Sevilla J M, Zaragoza G. Experimental characterization and optimization of multi-channel spiral wound air gap membrane distillation modules for seawater desalination. *Separation and Purification Technology*, 2018, 205: 212–222
 21. Mohamed E S, Boutikos P, Mathioulakis E, Belessiotis V. Experimental evaluation of the performance and energy efficiency of a vacuum multi-effect membrane distillation system. *Desalination*, 2017, 408: 70–80
 22. Drioli E, Ali A, Macedonio F. Membrane distillation: Recent developments and perspectives. *Desalination*, 2015, 356: 56–84
 23. Khayet M. Membranes and theoretical modeling of membrane distillation: a review. *Advances in Colloid and Interface Science*, 2011, 164(1–2): 56–88
 24. Martínez L, Florido-Díaz F J, Hernandez A, Prádanos P. Characterisation of three hydrophobic porous membranes used in membrane distillation: modelling and evaluation of their water vapour permeabilities. *Journal of Membrane Science*, 2002, 203(1–2): 15–27
 25. Izquierdo-Gil M A, García-Payo M C, Fernández-Pineda C. Air gap membrane distillation of sucrose aqueous solutions. *Journal of Membrane Science*, 1999, 155(2): 291–307
 26. Al-Obaidani S, Curcio E, Macedonio F, Di Profio G, Al-Hinai H, Drioli E. Potential of membrane distillation in seawater desalination: thermal efficiency, sensitivity study and cost estimation. *Journal of Membrane Science*, 2008, 323(1): 85–98
 27. Picard C, Larbot A, Guida-Pietrasanta F, Boutevin B, Ratsimihety A. Grafting of ceramic membranes by fluorinated silanes: hydrophobic features. *Separation and Purification Technology*, 2001, 25(1–3): 65–69
 28. Dafinov A, Garcia-Valls R, Font J. Modification of ceramic membranes by alcohol adsorption. *Journal of Membrane Science*, 2002, 196(1): 69–77
 29. Ko C C, Ali A, Drioli E, Tung K L, Chen C H, Chen Y R, Macedonio F. Performance of ceramic membrane in vacuum membrane distillation and in vacuum membrane crystallization. *Desalination*, 2018, 440: 48–58
 30. Chen X, Gao X, Fu K, Qiu M, Xiong F, Ding D, Cui Z, Wang Z, Fan Y, Drioli E. Tubular hydrophobic ceramic membrane with asymmetric structure for water desalination via vacuum membrane distillation process. *Desalination*, 2018, 443: 212–220
 31. Ali A, Macedonio F, Drioli E, Aljlil S, Alharbi O A. Experimental and theoretical evaluation of temperature polarization phenomenon in direct contact membrane distillation. *Chemical Engineering Research & Design*, 2013, 91(10): 1966–1977
 32. Drioli E, Giorno L, Fontananova E. *Comprehensive Membrane Science and Engineering*. 2nd ed. Oxford: Elsevier, 2017: 282–296
 33. Ravi J, Othman M H D, Matsuura T, Ro'ail Bilad M, El-badawy T H, Aziz F, Ismail A F, Rahman M A, Jaafar J. Polymeric membranes for desalination using membrane distillation: a review. *Desalination*, 2020, 490: 114530
 34. Yao M, Tijing L D, Naidu G, Kim S H, Matsuyama H, Fane A G, Shon H K. A review of membrane wettability for the treatment of saline water deploying membrane distillation. *Desalination*, 2020, 479: 114312
 35. Alkhudhiri A, Hilal N. *Emerging Technologies for Sustainable Desalination Handbook*. 1st ed. Oxford: Butterworth-Heinemann, 2018, 55–106
 36. Cohen Y. *Materials and Energy: Volume 17. Advances in Water Desalination Technologies*. Singapore: World Scientific Publishing Co. Pte. Ltd., 2021, 227–261
 37. Alhathal Alanezi A, Abdallah H, El-Zanati E, Ahmad A, Sharif A O. Performance investigation of O-ring vacuum membrane distillation module for water desalination. *Journal of Chemistry*, 2016: 9378460
 38. Gude G. *Emerging Technologies for Sustainable Desalination Handbook*. Burlington: Butterworth-Heinemann, 2018, 55–98
 39. Franken A C, Nolten J A, Mulder M H, Bargeman D, Smolders C A. Wetting criteria for the applicability of membrane distillation. *Journal of Membrane Science*, 1987, 33(3): 315–328
 40. Tijing L D, Woo Y C, Choi J S, Lee S, Kim S H, Shon H K. Fouling and its control in membrane distillation—a review. *Journal of Membrane Science*, 2015, 475: 215–244
 41. Rezaei M, Warsinger D M, Duke M C, Matsuura T, Samhaber W M. Wetting phenomena in membrane distillation: mechanisms, reversal, and prevention. *Water Research*, 2018, 139: 329–352
 42. Summers E K, Arafat H A, Lienhard J H. Energy efficiency comparison of single-stage membrane distillation (MD) desalination cycles in different configurations. *Desalination*, 2012, 290: 54–66
 43. Ding Z, Liu L, Li Z, Ma R, Yang Z. Experimental study of ammonia removal from water by membrane distillation (MD): the comparison of three configurations. *Journal of Membrane Science*, 2006, 286(1–2): 93–103
 44. Basile A. *Handbook of Membrane Reactors. Volume 2: Reactor Types and Industrial Applications*. 1st ed. Philadelphia: Woodhead Publishing, 2013, 78–81
 45. Bagger-Jørgensen R, Meyer A S, Varming C, Jonsson G. Recovery of volatile aroma compounds from black currant juice by vacuum membrane distillation. *Journal of Food Engineering*, 2004, 64(1): 23–31
 46. Wang L H, Pyatkovskyy T, Yousef A, Zeng X A, Sastry S K. Mechanism of *Bacillus subtilis* spore inactivation induced by moderate electric fields. *Innovative Food Science & Emerging Technologies*, 2020, 62: 102349
 47. Ali A, Quist-Jensen C A, Macedonio F, Drioli E. On designing of membrane thickness and thermal conductivity for large scale membrane distillation modules. *Journal of Membrane Science and Research*, 2016, 2(4): 179–185
 48. Wang P, Teoh M M, Chung T S. Morphological architecture of dual-layer hollow fiber for membrane distillation with higher desalination performance. *Water Research*, 2011, 45(17): 5489–

- 5500
49. Khayet M, Mengual J I, Matsuura T. Porous hydrophobic/hydrophilic composite membranes: application in desalination using direct contact membrane distillation. *Journal of Membrane Science*, 2005, 252(1–2): 101–113
 50. Deshmukh A, Elimelech M. Understanding the impact of membrane properties and transport phenomena on the energetic performance of membrane distillation desalination. *Journal of Membrane Science*, 2017, 539: 458–474
 51. Lawson K W, Loyd D R. Membrane distillation. *Journal of Membrane Science*, 1997, 24(1): 1–25
 52. Wang K Y, Foo S W, Chung T S. Mixed matrix PVDF hollow fiber membranes with nanoscale pores for desalination through direct contact membrane distillation. *Industrial & Engineering Chemistry Research*, 2009, 48(9): 4474–4483
 53. Eykens L, De Sitter K, Dotremont C, Pinoy L, Van der Bruggen B. How to optimize the membrane properties for membrane distillation: a review. *Industrial & Engineering Chemistry Research*, 2016, 55(35): 9333–9343
 54. Schneider K, Hölz W, Wollbeck R, Ripperger S. Membranes and modules for transmembrane distillation. *Journal of Membrane Science*, 1988, 39(1): 25–42
 55. Tang Y, Li N, Liu A, Ding S, Yi C, Liu H. Effect of spinning conditions on the structure and performance of hydrophobic PVDF hollow fiber membranes for membrane distillation. *Desalination*, 2012, 287: 326–339
 56. Gryta M. Fouling in direct contact membrane distillation process. *Journal of Membrane Science*, 2008, 325(1): 383–394
 57. Du H, Li J, Zhang J, Su G, Li X, Zhao Y. Separation of hydrogen and nitrogen gases with porous graphene membrane. *Journal of Physical Chemistry C*, 2011, 115(47): 23261–23266
 58. Basile A, Cassano A, Rastogi N K. *Advances in Membrane Technologies for Water Treatment: Materials, Processes and applications*. 1st ed. Cambridge: Woodhead Publishing, 2015, 605–624
 59. Lin J C, Lee D J, Huang C. Membrane fouling mitigation: membrane cleaning. *Separation Science and Technology*, 2010, 45(7): 858–872
 60. Norafifah H, Noordin M Y, Wong K Y, Izman S, Ahmad A A. A study of operational factors for reducing the fouling of hollow fiber membranes during wastewater filtration. *Procedia CIRP*, 2015, 26: 781–785
 61. Shakharamipour N, Tran T N, Ramanan S, Lin H. Membranes with surface-enhanced antifouling properties for water purification. *Membranes*, 2017, 7(1): 13
 62. Teoh M M, Chung T S, Yeo Y S. Dual-layer PVDF/PTFE composite hollow fibers with a thin macrovoid-free selective layer for water production via membrane distillation. *Chemical Engineering Journal*, 2011, 171(2): 684–691
 63. Teoh M M, Chung T S. Membrane distillation with hydrophobic macrovoid-free PVDF-PTFE hollow fiber membranes. *Separation and Purification Technology*, 2009, 66(2): 229–236
 64. Zou L, Gusnawan P, Jiang Y B, Zhang G, Yu J. Macrovoid-inhibited PVDF hollow fiber membranes via spinning process delay for direct contact membrane distillation. *ACS Applied Materials & Interfaces*, 2020, 12(25): 28655–28668
 65. Mansourizadeh A, Ismail A F. Hollow fiber gas-liquid membrane contactors for acid gas capture: a review. *Journal of Hazardous Materials*, 2009, 171(1–3): 38–53
 66. Drioli E, Giorno L. *Encyclopedia of Membranes*. 1st ed. Berlin: Springer, 2016, 1009–1012
 67. Schofield R W, Fane A G, Fell C J. Gas and vapour transport through microporous membranes. I. Knudsen-Poiseuille transition. *Journal of Membrane Science*, 1990, 53(1–2): 159–171
 68. Guijt C M, Meindersma G W, Reith T, De Haan A B. Air gap membrane distillation: 2. Model validation and hollow fibre module performance analysis. *Separation and Purification Technology*, 2005, 43(3): 245–255
 69. McGaughey A L, Gustafson R D, Childress A E. Effect of long-term operation on membrane surface characteristics and performance in membrane distillation. *Journal of Membrane Science*, 2017, 543: 143–150
 70. Gryta M. Long-term performance of membrane distillation process. *Journal of Membrane Science*, 2005, 265(1–2): 153–159
 71. Srisurichan S, Jiraratananon R, Fane A G. Mass transfer mechanisms and transport resistances in direct contact membrane distillation process. *Journal of Membrane Science*, 2006, 277(1–2): 186–194
 72. Martínez-Diez L, Vazquez-Gonzalez M I. Temperature and concentration polarization in membrane distillation of aqueous salt solutions. *Journal of Membrane Science*, 1999, 156(2): 265–273
 73. Asghari M, Dehghani M, Riasat Harami H, Mohammadi A H. Effects of operating parameters in sweeping gas membrane distillation process: numerical simulation of Persian Gulf seawater desalination. *Journal of Water and Environmental Nanotechnology*, 2018, 3(2): 128–140
 74. Ali A, Quist-Jensen C A, Macedonio F, Drioli E. Optimization of module length for continuous direct contact membrane distillation process. *Chemical Engineering and Processing*, 2016, 110: 188–200
 75. Ali A, Tsai J H, Tung K L, Drioli E, Macedonio F. Designing and optimization of continuous direct contact membrane distillation process. *Desalination*, 2018, 426: 97–107
 76. Cerci Y. Exergy analysis of a reverse osmosis desalination plant in California. *Desalination*, 2002, 142(3): 257–266
 77. Macedonio F, Curcio E, Drioli E. Integrated membrane systems for seawater desalination: energetic and exergetic analysis, economic evaluation, experimental study. *Desalination*, 2007, 203(1–3): 260–276
 78. Macedonio F, Drioli E. An exergetic analysis of a membrane desalination system. *Desalination*, 2010, 261(3): 293–299
 79. Macedonio F, Criscuoli A, Gzara L, Albeirutty M, Drioli E. Water and salts recovery from desalination brines: an exergy evaluation. *Journal of Environmental Chemical Engineering*, 2021, 9(5): 105884
 80. Drioli E, Curcio E, Di Profio G, Macedonio F, Criscuoli A. Integrating membrane contactors technology and pressure-driven membrane operations for seawater desalination: energy, exergy and costs analysis. *Chemical Engineering Research & Design*, 2006, 84(3): 209–220
 81. Shukuya M, Hammache A. Introduction to the concept of exergy-

- for a better understanding of low-temperature-heating and high-temperature-cooling systems. VTT Technical Research Centre of Finland, VTT Tiedotteita—Research Notes No. 2158, 2002, 1–61
82. Ali A, Quist-Jensen C A, Drioli E, Macedonio F. Evaluation of integrated microfiltration and membrane distillation/crystallization processes for produced water treatment. *Desalination*, 2018, 434: 161–168
83. Tufa R A, Noviello Y, Di Profio G, Macedonio F, Ali A, Drioli E, Fontananova E, Bouzek K, Curcio E. Integrated membrane distillation-reverse electro dialysis system for energy-efficient sea-water desalination. *Applied Energy*, 2019, 253: 113551
84. Perrotta M L, Saielli G, Casella G, Macedonio F, Giorno L, Drioli E, Gugliuzza A. An ultrathin suspended hydrophobic porous membrane for high-efficiency water desalination. *Applied Materials Today*, 2017, 9: 1–9
85. Eykens L, Hitsov I, De Sitter K, Dotremont C, Pinoy L, Nopens I, Van der Bruggen B. Influence of membrane thickness and process conditions on direct contact membrane distillation at different salinities. *Journal of Membrane Science*, 2016, 498: 353–364
86. Woo Y C, Tijing L D, Shim W G, Choi J S, Kim S H, He T, Drioli E, Shon H K. Water desalination using graphene-enhanced electrospun nanofiber membrane via air gap membrane distillation. *Journal of Membrane Science*, 2016, 520: 99–110
87. Celebi K, Buchheim J, Wyss R M, Droudian A, Gasser P, Shorubalko I, Kye J I, Lee C, Park H G. Ultimate permeation across atomically thin porous graphene. *Science*, 2014, 344(6181): 289–292
88. Mi B. Graphene oxide membranes for ionic and molecular sieving. *Science*, 2014, 343(6172): 740–742
89. Surwade S P, Smirnov S N, Vlasiouk I V, Unocic R R, Veith G M, Dai S, Mahurin S M. Water desalination using nanoporous single-layer graphene. *Nature Nanotechnology*, 2015, 10(5): 459–464
90. Balandin A A, Ghosh S, Bao W, Calizo I, Teweldebrhan D, Miao F, Lau C N. Superior thermal conductivity of single-layer graphene. *Nano Letters*, 2008, 8(3): 902–907
91. Ho C Y, Powell R W, Liley P E. Thermal conductivity of the elements. *Journal of Physical and Chemical Reference Data*, 1972, 1(2): 279–421
92. Grasso G, Galiano F, Yoo M J, Mancuso R, Park H B, Gabriele B, Figoli A, Drioli E. Development of graphene-PVDF composite membranes for membrane distillation. *Journal of Membrane Science*, 2020, 604: 118017
93. Woo Y C, Kim Y, Shim W G, Tijing L D, Yao M, Nghiem L D, Choi J S, Kim S H, Shon H K. Graphene/PVDF flat-sheet membrane for the treatment of RO brine from coal seam gas produced water by air gap membrane distillation. *Journal of Membrane Science*, 2016, 513: 74–84
94. Gontarek E, Macedonio F, Militano F, Giorno L, Lieder M, Politano A, Drioli E, Gugliuzza A. Adsorption-assisted transport of water vapour in super-hydrophobic membranes filled with multi-layer graphene platelets. *Nanoscale*, 2019, 11(24): 11521–11529
95. Frappa M, Castillo A D, Macedonio F, Politano A, Drioli E, Bonaccorso F, Pellegrini V, Gugliuzza A. A few-layer graphene for advanced composite PVDF membranes dedicated to water desalination: a comparative study. *Nanoscale Advances*, 2020, 2(10): 4728–4739
96. Gugliuzza A, Macedonio F, Politano A, Drioli E. Prospects of 2D materials-based membranes in water desalination. *Chemical Engineering Transactions*, 2019, 73: 265–270
97. Macedonio F, Politano A, Drioli E, Gugliuzza A. Bi₂Se₃-assisted membrane crystallization. *Materials Horizons*, 2018, 5(5): 912–919
98. Frappa M, Macedonio F, Gugliuzza A, Jin W, Drioli E. Performance of PVDF based membrane with 2D materials for Membrane Assisted-Crystallization process. *Membranes*, 2021, 11(5): 302
99. Krupenkin T N, Taylor J A, Schneider T M, Yang S. From rolling ball to complete wetting: the dynamic tuning of liquids on nanostructured surfaces. *Langmuir*, 2004, 20(10): 3824–3827
100. Saffarini R B, Mansoor B, Thomas R, Arafat H A. Effect of temperature-dependent microstructure evolution on pore wetting in PTFE membranes under membrane distillation conditions. *Journal of Membrane Science*, 2013, 429: 282–294
101. Yin Y, Jeong N, Tong T. The effects of membrane surface wettability on pore wetting and scaling reversibility associated with mineral scaling in membrane distillation. *Journal of Membrane Science*, 2020, 614: 118503
102. Gryta M. The application of polypropylene membranes for production of fresh water from brines by membrane distillation. *Chemical Papers*, 2017, 71(4): 775–784
103. Meng S, Ye Y, Mansouri J, Chen V. Fouling and crystallisation behaviour of superhydrophobic nano-composite PVDF membranes in direct contact membrane distillation. *Journal of Membrane Science*, 2014, 463: 102–112
104. Srisurichan S, Jiratananon R, Fane A G. Humic acid fouling in the membrane distillation process. *Desalination*, 2005, 174(1): 63–72
105. Lu K J, Chung T S. *Membrane Distillation: Membranes, Hybrid Systems and Pilot Studies*. Boca Raton: CRC Press, 2019, 167–182
106. Razmjou A, Arifin E, Dong G, Mansouri J, Chen V. Superhydrophobic modification of TiO₂ nanocomposite PVDF membranes for applications in membrane distillation. *Journal of Membrane Science*, 2012, 415: 850–863
107. Ma Z, Hong Y, Ma L, Su M. Superhydrophobic membranes with ordered arrays of nanospiked microchannels for water desalination. *Langmuir*, 2009, 25(10): 5446–5450
108. Su C, Horseman T, Cao H, Christie K, Li Y, Lin S. Robust superhydrophobic membrane for membrane distillation with excellent scaling resistance. *Environmental Science & Technology*, 2019, 53(20): 11801–11809
109. Lin S, Nejati S, Boo C, Hu Y, Osuji C O, Elimelech M. Omniphobic membrane for robust membrane distillation. *Environmental Science & Technology Letters*, 2014, 1(11): 443–447
110. Lu K J, Zuo J, Chang J, Kuan H N, Chung T S. Omniphobic hollow-fiber membranes for vacuum membrane distillation. *Environmental Science & Technology*, 2018, 52(7): 4472–4480
111. Woo Y C, Chen Y, Tijing L D, Phuntsho S, He T, Choi J S, Kim S H, Shon H K. CF₄ plasma-modified omniphobic electrospun nanofiber membrane for produced water brine treatment by membrane distillation. *Journal of Membrane Science*, 2017, 529: 234–242
112. Yang H C, Hou J, Chen V, Xu Z K. Janus membranes: exploring duality for advanced separation. *Angewandte Chemie International*

- Edition, 2016, 55(43): 13398–13407
113. Chen Y, Lu K J, Japip S, Chung T S. Can composite Janus membranes with an ultrathin dense hydrophilic layer resist wetting in membrane distillation? *Environmental Science & Technology*, 2020, 54(19): 12713–12722
 114. Timin A S, Gao H, Voronin D V, Gorin D A, Sukhorukov G B. Inorganic/organic multilayer capsule composition for improved functionality and external triggering. *Advanced Materials Interfaces*, 2017, 4(1): 1600338
 115. Shi H, He Y, Pan Y, Di H, Zeng G, Zhang L, Zhang C. A modified mussel-inspired method to fabricate TiO₂ decorated superhydrophilic PVDF membrane for oil/water separation. *Journal of Membrane Science*, 2016, 506: 60–70
 116. McKeen L W. *Permeability Properties of Plastics and Elastomers*. 3rd ed. Waltham: Elsevier, 2012, 21–37
 117. Tsai J H, Perrotta M L, Gugliuzza A, Macedonio F, Giorno L, Drioli E, Tung K L, Tocci E. Membrane-assisted crystallization: a molecular view of NaCl nucleation and growth. *Applied Sciences (Basel, Switzerland)*, 2018, 8(11): 2145
 118. Whelan A. *Polymer Technology Dictionary*. 1st ed. London: Springer Science & Business Media, 2012, 341
 119. Bottino A, Capannelli G, Munari S, Turturro A. High performance ultrafiltration membranes cast from LiCl doped solutions. *Desalination*, 1988, 68(2–3): 167–177
 120. Mansourizadeh A, Ismail A F. Effect of LiCl concentration in the polymer dope on the structure and performance of hydrophobic PVDF hollow fiber membranes for CO₂ absorption. *Chemical Engineering Journal*, 2010, 165(3): 980–988
 121. Chen S, Ishii J, Horiuchi S, Yoshizawa-Fujita M, Izgorodina E I. Difference in chemical bonding between lithium and sodium salts: influence of covalency on their solubility. *Physical Chemistry Chemical Physics*, 2017, 19(26): 17366–17372